Experimental Determination of the Landé g-factor for Diphenylpicrylhydrazyl (DPPH) via Electron Spin Resonance

Ezra E. Brajcic[1] and Julia Parker[2]
Department of Physics, University of Guelph
Guelph, Ontario, N1G 2W1, Canada

(Dated: March 17, 2025)

[1]Email: ebrajcic@uoguelph.ca
[2]Email: jparke10@uoguelph.ca

Abstract

The Landé g-factor, a critical parameter in quantifying the magnetic moment of electrons, was experimentally determined for the stable organic radical diphenylpicrylhydrazyl (DPPH) using electron spin resonance (ESR) spectroscopy. DPPH's chemical stability and quenched orbital angular momentum make it an ideal candidate for precise g-factor measurements in simplified laboratory setups. Our experiment utilized two distinct measurement approaches: direct probe signal analysis and lock-in amplifier signal processing. We established the relationship between resonant frequencies ($90-180$MHz) and corresponding magnetic field strengths using Helmholtz coils with variable offset voltages. The experimental apparatus was carefully calibrated and optimized to account for thermal effects and signal sensitivity. Through orthogonal distance regression analysis, we determined isotropic g-factor values of 2.003 ± 0.017 and 1.999 ± 0.053, consistent with the accepted value of 2.0036, differing by 0.029% and 0.23%, respectively. Additionally, we developed a GPU-accelerated computational model to visualize the spin density distribution throughout the DPPH molecule, confirming the delocalization of the unpaired electron. The study underscores ESR's effectiveness in undergraduate laboratories despite equipment constraints and proposes future enhancements, including improved cooling systems and microelectromechanical sensors. Bridging experimental and computational methodologies, this work advances the understanding of quantum mechanical properties in molecular systems and reinforces ESR's pedagogical value in physics education.

1 Introduction and Theory

The electron g-factor (g_e), also known as the Landé g-factor, is one of the most precisely measured quantities in physics and its determination was a triumph for physicists in the mid-twentieth century, validating the theory of quantum electrodynamics (QED). Its value for the free electron $g_e = 2.0023930436092(27)$[3], is a proportionality constant for its magnetic moment and corrects the originally theorized value known as the Bohr magneton (μ_B). While it's most famous for its confirmation of QED[3], it also plays a key role in atomic physics, primarily through a phenomenon called spin-orbit coupling (SOC).[4][8] SOC occurs in atomic bound states that are under the influence of an external magnetic field where the orbital angular momentum $\vec{L}$ and intrinsic spin angular momentum $\vec{S}$ add together to form the total angular momentum $\vec{J} = \vec{L} + \vec{S}$. This coupling breaks the energy degeneracy in atomic energy states and allows electrons to take on more energy levels than before and explains the splitting of spectral lines in atoms known as the Zeeman effect.[4][8] Given its wide range of applications, the experimental determination of the electron g-factor remains critical in developing our understanding of physics.

One commonly used method of measurement for the Landé g-factor is electron paramagnetic resonance (ESR) spectroscopy where materials are exposed to a constant magnetic field which induces a torque on the electrons that comprise it, causing them to either align parallel or anti-parallel to the magnetic field's direction.[1][11] This is demonstrated by solving the time-dependent Schrödinger equation for the free electron at rest. Under a magnetic field $B_0\hat{z}$ an electron experiences a torque equivalent to $\vec{\tau} = \vec{\mu} \times \vec{B}$, and a potential $U = -\vec{\mu} \cdot \vec{B}$, where $\vec{\mu} = g_e \frac{\mu_B}{\hbar} \vec{S}$, and $\mu_B = \frac{e\hbar}{2m_e}$. The expression for the magnetic moment can be further condensed into $\vec{\mu} = \gamma_e \vec{S}$, the gyromagnetic ratio which will come into play later. The Hamiltonian can then be represented as

$$\mathcal{H}_0 = -\gamma_e B_0 \frac{\hbar}{2} \begin{pmatrix} 1 & 0 \\ 0 & -1 \end{pmatrix}. \tag{1.1}$$

Which can then be substituted into the time-dependent Schrödinger equation.

$$-i\hbar \frac{\partial}{\partial t} |\psi(t)\rangle = \mathcal{H}_0 |\psi(0)\rangle \tag{1.2}$$

This leads to the general solution

$$|\psi(t)\rangle = e^{-i\mathcal{H}_0 t/\hbar} |\psi(0)\rangle ,$$

and since the matrix in (Eq. 1.1) is already diagonalized we know its energy eigenstates to be

$$E_\pm = \mp \gamma_e B_0 \frac{\hbar}{2}. \tag{1.3}$$

Which are respectively aligned parallel and anti-parallel to the magnetic field. Therefore, for the initial spin state

$$|\psi(0)\rangle = \begin{pmatrix} a \\ b \end{pmatrix},$$

the time evolving state becomes

$$|\psi(t)\rangle = \begin{pmatrix} a e^{i\gamma_e B_0/2} \\ b e^{-i\gamma_e B_0/2} \end{pmatrix}.$$

Since we chose to use the z-basis the electron precesses at a constant angle $a = \cos(\alpha/2)$ and $b = \sin(\alpha/2)$ to the z-axis because only a single spin direction can be known from any measurement and the probability of either state must be normalized to $|a|^2 + |b|^2 = 1$. The rate of this precession is exactly $\omega_0 = -\gamma_e B_0$, known as the Larmor frequency[4].

If one were to apply a time-dependent perturbation to this system. The electron can be induced into transitioning to the higher energy eigenstate if the perturbation is of the same energy as the difference in the energy between the eigenstates, this condition is the foundation of ESR spectroscopy[1][11] and can be fulfilled by an electromagnetic wave with a frequency corresponding to

$$h\omega = \Delta E = \gamma_e B_0 \hbar, \tag{1.4}$$

which can also be represented as

$$h\omega = \Delta E = g_e \mu_B B_0. \tag{1.5}$$

The aforementioned is the characteristic equation used in ESR experiments. By matching the frequency of the electromagnetic wave with a magnetic field of proportional magnitude to the difference in the free electron's lower energy eigenstate, a resonance effect occurs and the incident electromagnetic radiation is absorbed.[1][11]

From time-dependent perturbation theory, assuming that the wavelength of an incident electromagnetic wave is much larger than the space that the electron is free to move within, a magnetic dipole potential can be applied to the original Hamiltonian in (Eq. 1.1)[4]

$$\mathcal{H}' = -\gamma_e B_\omega \frac{\hbar}{2} \cos(\omega t) \begin{pmatrix} 1 & 0 \\ 0 & -1 \end{pmatrix} \tag{1.6}$$

$$\mathcal{H} = \mathcal{H}_0 + \mathcal{H}'$$

$$\mathcal{H} = \frac{-\gamma_e \hbar}{2} (B_0 + B_\omega \cos(\omega t)) \begin{pmatrix} 1 & 0 \\ 0 & -1 \end{pmatrix} \tag{1.7}$$

Again, like (Eq. 1.1), since the Hamiltonian is already diagonalized, it's energy eigenstates are known to be

$$E_\pm = \mp \gamma_e \frac{\hbar}{2} (B_0 + B_\omega \cos(\omega t)).$$

These correspond to the following set of differential equations due to the time-dependent Schrödinger equation (Eq. 1.2).

$$\dot{c}_+(t) = c_+(0) e^{i\gamma_e (B_0 + B_\omega \cos(\omega t))/2}$$

$$\dot{c}_-(t) = c_-(0) e^{-i\gamma_e (B_0 + B_\omega \cos(\omega t))/2}$$

After applying simple integration to each equation and applying the initial spin conditions

$$c_+(t) = c_+(0) e^{\frac{i\gamma_e}{2\omega}(B_0 \omega t + B_\omega \sin(\omega t))}, \tag{1.8}$$

$$c_-(t) = c_-(0) e^{-\frac{i\gamma_e}{2\omega}(B_0 \omega t + B_\omega \sin(\omega t))}, \tag{1.9}$$

we can conclude that if the electron happened to not be in a mixed state it would never be able to make any energy transitions, even after being perturbed. Therefore a periodic perturbation transverse to the original that also interacts with the electron's intrinsic spin is required. A scalar potential field or a potential diagonalized to the chosen spin basis will only change the phase factor of the wave function.[1][4][11]

It is also important to consider the relative quantity of spin states in the sample material being studied, this is described using a Boltzmann distribution[4]

$$\frac{N_{E+}}{N_{E-}} = e^{-\frac{\Delta E}{kT}} = e^{-\frac{h\omega}{kT}}. \tag{1.10}$$

Where k is the Boltzmann Constant and T is the temperature of the sample in kelvin. The equation represents the equilibrium point between absorption, stimulated emission, and spontaneous emission. If neither stimulated emission or spontaneous emission are present, the population of higher energy eigenstates in the system increases until every possible excited state becomes saturated and no resonance signal could be detected.[4]

DPPH presents itself as a prime candidate for measuring the Landé g-factor in this experiment due to its high physical and chemical stability, making it an ideal benchmark for comparison in ESR spectroscopy experiments. The unpaired electron present in the molecule has a quenched orbital angular momentum, allowing for precise determination of the Landé g-factor for the free electron with relative ease.[5] This makes DPPH especially useful in undergraduate labs, as it eliminates the need for expensive equipment such as vacuum chambers, electromagnets, and magnetic traps typically required to measure the Landé g-factor of free electrons.[3] Its properties simplify experimental setups while maintaining accuracy, making it an excellent material for foundational ESR studies.

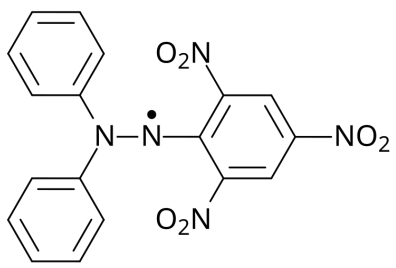

Figure 1: *Chemical Structure of diphenylpicrylhydrazyl (DPPH) radical.*

2 Physical Analysis of DPPH

Diphenylpicrylhydrazyl (DPPH) is a stable, organic, radical, chemical compound. Using molecular orbital theory, one can notice that the unpaired electron in DPPH participates in a π-bond which has a quantum angular orbital momentum number $L = 1$. Despite this, the accepted value of the Landé g-factor for the unpaired electron is $g = 2.0036$[5], very close to the accepted value for the free electron. This is due to a phenomenon called orbital quenching, where $\vec{L} \approx 0$ due to the electron being delocalized throughout the entire molecule.

Building off of J. X. Boucherle et al. (1986), it is possible to map the probability density also known as spin density of the radical in its solid, crystalline form through a linear combination of Slater-type orbitals (STO)s that also account for multipole expansions.[6]

$$\rho_s(r) = \sum_{atoms} \sum_{l=0}^{\infty} \sum_{m=-l}^{l} P_{lm}\rho_{lm}(r) \qquad (2.1)$$

P_{lm} are the multipole populations determined by neutron diffraction measurements of a DPPH crystal[6] and $\rho_{lm}(r)$ represents the product of an STO with a real spherical harmonic corresponding to the l and m quantum numbers defined as

$$\rho_{lm}(r) = \frac{\zeta^{n_l+3}}{(n_l+2)!} r^{n_l} e^{-\zeta r} Y_l^m(\hat{r}). \qquad (2.2)$$

Where ζ is a fitted scaling term and n_l represents the exponents of the radial functions, $n_l = 2$ is applied to monopole as well as dipole terms, and $n_l = 3$ for quadropole terms[6].

It is then possible to observe each atom's contribution to the spin density of the DPPH molecule, both qualitatively and quantitatively given the accuracy of the model used. This was accomplished by programming (Eq. 2.1) and (Eq. 2.2) in Python for an entire molecule of DPPH. To take advantage of GPU-accelerated computing, the program was designed to execute on a Nvidia RTX 3070 graphics processing unit (GPU). Additionally, parallel processing concepts such as chunking and dynamic memory management were applied. Interfacing with the GPU was achieved through the CuPy Python library which communicates to Compute Unified Device Architecture (CUDA), a proprietary application programming interface (API) to directly interface with the GPU's instruction set. This reduced the estimated computation time from over 24 hours to mere seconds. The code used to analyze the spin density of DPPH is linked in the appendix.

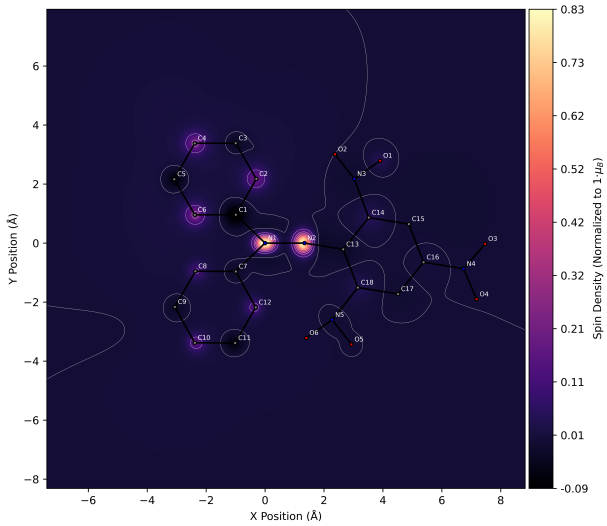

(a) $z = 0.0Å$

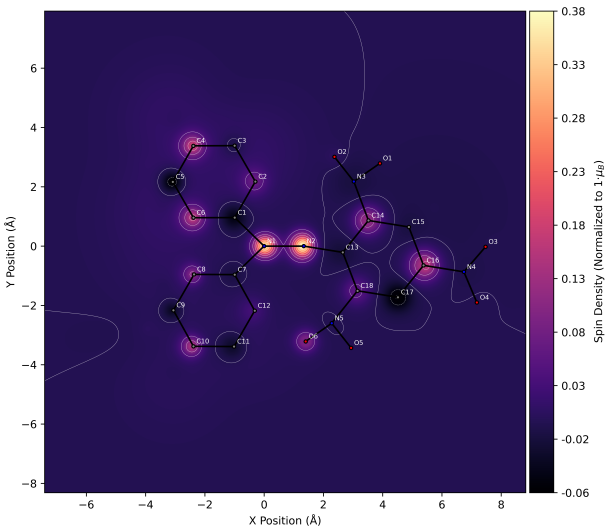

(b) $z = -0.5Å$

Figure 2: *Spin density heatmaps and contour plots of DPPH shown in its planar form for better visualization and normalized to* $1\mu_B$*, (a) at* $z = 0Å$*, with a contour interval of* $0.092\mu_B$*, and (b) at* $z = -0.5Å$*, with a contour interval of* $0.044\mu_B$

From observation, it is clear that the electron is essentially free to move throughout the entire molecule and that the probability density matches DPPH's possible resonance structures, including the anisotropic one about the C_1 phenyl group observed in figure 2[5]. When measuring the Landé g-factor of DPPH via ESR, the value determined is, in reality, an effective g-factor that changes the incident, constant magnetic field used in ESR experiments to[1][11]

$$B_0 \rightarrow B_{eff} = (1-\sigma)B_0 = \frac{g}{g_e}B_0.$$

The characteristic equation (Eq. 1.4) then becomes

$$h\omega = \Delta E = g\mu_B B_0. \tag{2.3}$$

This is due to a multitude of effects such as SOC, the hyperfine interaction, crystal structure, etc.[1][11] Some of these factors lead to anisotropy in the Landé g-factor where it becomes a tensor of the form

$$g^T = \begin{pmatrix} g_{xx} & g_{xy} & g_{xz} \\ g_{yx} & g_{yy} & g_{yz} \\ g_{zx} & g_{zy} & g_{zz} \end{pmatrix}. \tag{2.4}$$

These anisotropic values can be measured by varying the direction of the magnetic field or rotating the crystal, though, in the case of DPPH, it remains highly isotropic up until resonant frequencies of ~ 200GHz.[10]

3 Apparatus Assembly

The apparatus for generating paramagnetic resonant states in DPPH employs two Helmholtz coils that produce a uniform 35 Hz magnetic field. Field strength is controlled by sending an offset voltage from a computer—via a National Instruments interface box (NIIB) and the Labview ESR app—to an LM12 AC amplifier, which is tuned to deliver maximum current without saturating the coils. Cooling is achieved with heat sinks attached to the coils and a 120 mm, 15 V DC fan that increased airflow. A radio frequency generator was used to induce a spin flip transitions in the DPPH sample. For this experiment, a Hewlett Packard 8647A signal generator was employed within a frequency range of 10-180 MHz. For this frequency range, the generator must have an extremely low output signal noise level for the resonance absorption signal to be detectable. When considering the DPPH sample as a Boltzmann distribution, from (Eq. 1.10)[4], the relative number of spin states influenced by a transverse electromagnetic wave within this frequency range differs only slightly at room temperature (~ $20C°$). Specifically, the difference is 0.0014% at ~ 90 MHz and increases to 0.0029% at ~ 180 MHz. Therefore the absorption signal is extremely small. The RF signal enters an LRC resonance circuit, where crystalline DPPH powder is placed within the inductor—positioned normal to the Helmholtz coils—to permit mixed spin states as proved by (Eq. 1.8) and (Eq. 1.9)[1][4][11]. A variable probe capacitor within the LRC circuit is tuned to amplify the absorption signal for each resonant offset voltage measurement performed by connecting the capacitor to a Philips PM 3050 50 MHz oscilloscope and adjusting it via a screwdriver until a minimum voltage reading is achieved. Finally, the circuit connects to a diode (oriented against the input signal so only the negative portion passes) and a preceding capacitor further amplifies the signal.

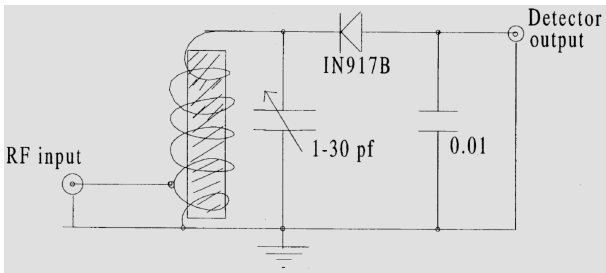

Figure 3: *ESR probe circuit diagram, comprised of LRC circuit with variable capacitor, diode, and fixed capacitor*

Two sets of measurements were carried out to determine the Landé g-factor were performed, each using a different method in the final step in absorbance signal amplification. In the first set of measurements, the signal produced by the probe was sent directly to the computer interfacing with the NIIB. For the

second set of Landé g-factor measurements, the signal was sent to a Stanford Research Systems SR510 lock-in amplifier with a 35Hz reference signal and then sent to the computer utilizing the same method. However, the output signal from the lock-in amplifier represents the first derivative of the absorption signal rather than the actual absorption signal.

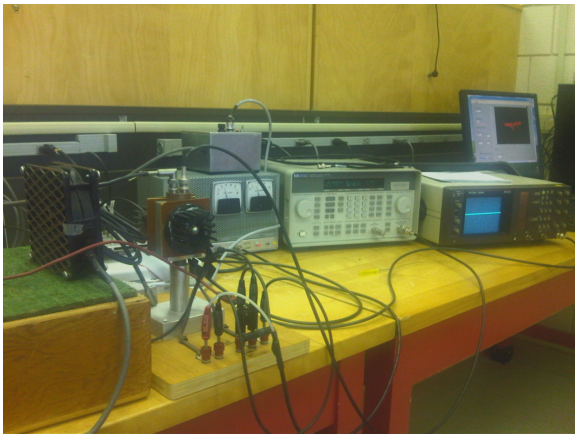

(a)

(b)

Figure 4: *(a) Image of apparatus used for first set of Landé g-factor measurements with LM12 AC amplifier. (b) Image of apparatus used in second set of Landé g-factor measurements with Stanford Research Systems SR510 lock-in amplifier.*

Due to department budget constraints, a Gaussmeter and variable probe capacitor were not able to be installed directly by the DPPH sample and were instead placed on top of the DPPH sample casing. Probes would be swapped out and replaced by one another as needed. This also had the consequence that the calibration measurements for the effective magnetic field at resonance points had to be done beforehand for both sets of measurements.

4 Methodology

4.1 Magnetic Field Measurements

Before calibration, the W Bell 5180 Gaussmeter used was itself calibrated to maximize the magnitude of the measured magnetic field. Calibration measurements were performed to determine the effective magnetic field near the DPPH sample for both sets of Landé g-factor measurements. This was accomplished by sending offset voltage signals ranging from 1.00-10.00V in 1.00V increments to the Helmholtz coils via the Labview ESR app. Measurements were repeated to mitigate high variability, with uncertainties determined from the average deviation of the time-averaged readings Fast recording was essential, as higher offset voltages caused rapid temperature increases in the coils. While the Gaussmeter itself had an intrinsic uncertainty, it was far less than any time averaged uncertainties. It was also assumed that the offset voltages output by the computer had a negligible uncertainty

4.2 Direct Probe Signal Measurements

After calibration, the Gaussmeter was removed and the variable capacitor positioned atop the DPPH casing. With the RF generator active and the offset voltage set to 0.00V, the Labview app was used to adjust the phase until the two negative signal amplitudes aligned at the origin. Resonant frequencies were measured over the 90-180 MHz range in 10.00000 MHz increments. Frequency uncertainties are negligible in this case as the Hewlett Packard 8647A signal generator is precise in its set frequency down to a single Hertz. For each resonant frequency measurement, the variable capacitor was re-calibrated and a corresponding offset voltage for the Helmholtz coils was found by varying the offset voltage in the Labview app until the peak of the absorption signal was at the origin V=0.00. This corresponding offset voltage represents the resonance point from (Eq. 2.3). When a resonance condition is satisfied, the magnetic field stored in the

inductor around the DPPH sample is depleted and the impedance drops noticeably, leading to a large increase in the magnitude of the negative output voltage reading. Zeroing in the absorbance signal onto the origin of the Labview app display maximizes it's amplitude and therefore, reaches a resonance state. Since heating causes the required offset voltage to drift over time, an initial guess was made; if off-target, the offset was reset to 0.00V and measurements paused for about 90 seconds to allow the coils to cool before re-adjustment. However, since the resonance voltage was constantly shifting and the observed absorption signal had a significant amount of noise, a uncertainty was added to the voltage corresponding to it's average shift

4.3 Lock-in Amplifier Signal Measurements

For the second measurement set, care was taken to keep the lock-in amplifier off during connections to protect its circuitry. Prior to activation, the RF generator was set to a resonant frequency and the variable capacitor tuned as before. Once the capacitor was switched from the oscilloscope to the lock-in amplifier, the device was turned on and it's sensitivity was tuned, ensuring that the signal output was within the range of the computer's voltage input. The Helmholtz coils' offset voltage was then swept continuously from 1.00-10.00V over 180 seconds via the Labview app, which logged both the signal amplitude and offset voltage data in a .lvm file. After data acquisition, the process was repeated over the same frequency range of 90-180 MHz in 10.00000 MHz increments, turning the lock-in amplifier off, re-calibrating the capacitor, and re-tuning the lock-in amplifier as necessary before recording data for the next frequency. For the duration of the experiment, it was found that a lock-in amplifier sensitivity of 20mV sufficed.

4.4 Data Analysis

Due to the methods of measurement used, both the magnetic field strength and resonant frequency become linear functions of voltage, this permitted the use of linear regression to create functions for the two components of (Eq. 2.3) and then rearranging the equation to solve for the Landé g-factor.

For the second set of measurements, the same form of linear regression was carried out on the magnetic field calibration data. However, the .lvm files need to be parsed through to find the x-intercept of each signal as the x-intercept of the first derivative corresponds to the maximum amplitude of the absorption signal.[1][11] Additionally, there were still small time-steps present in the data so to get a better approximation for the x-intercept point, a linear slope function was made between the two amplitude readings present just before and just after the function passes through the x-axis. The intercept of this slope is what was used to find the resonance voltage. Uncertainties for both sets of measurements were propagated via commonly used formulas and approximations.

All functions for the magnetic field strength and offset voltage relation were generated via weighted linear regression due to uncertainties only being present in the dependent variable. Functions for the frequency and offset voltage relation as well as the Landé g-factor were obtained through orthogonal distance regression (ODR). Additionally, linear regression of the data without error terms was used to provide the ODR algorithm with an initial parameter estimate. All methods used in the data analysis were programmed using Python with the SciPy and Matplotlib libraries for regression and plotting respectively. Though, for ODR, numerical instability necessitated normalization of the data before regression as well as the manual computing for the covariance. The code and data used in the analysis is linked the appendix.

5 Results

During calibration measurements for the magnetic field for both determination methods of the Landé g-factor, a time averaged uncertainty in the magnetic field strength of ±0.2G

was found for all measurements. Additionally, at higher voltages, the linear relationship between the offset voltage and magnetic field strength broke down likely due to the increased resistance of the Helmholtz coils as their temperature increased. Because of this, calibration measurements at offset voltages of 8.00, 9.00, and 10.00V for the first determination as well as 9.00V and 10.00V for the second determination were discarded as outliers. Removing these values does not affect any frequency measurements taken as none of the resonant frequencies used had corresponding offset voltages larger than the offset voltages used in the magnetic field calibration measurements.

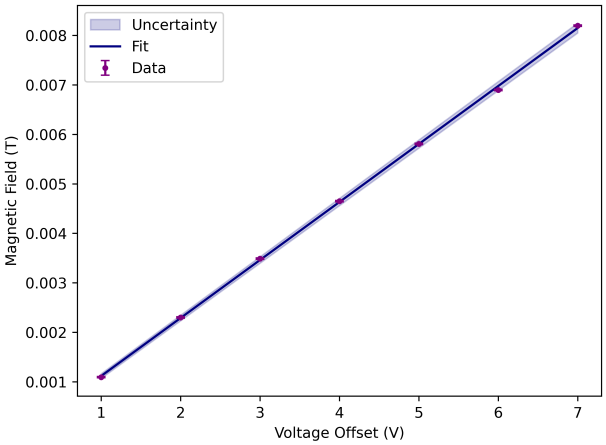

(a)

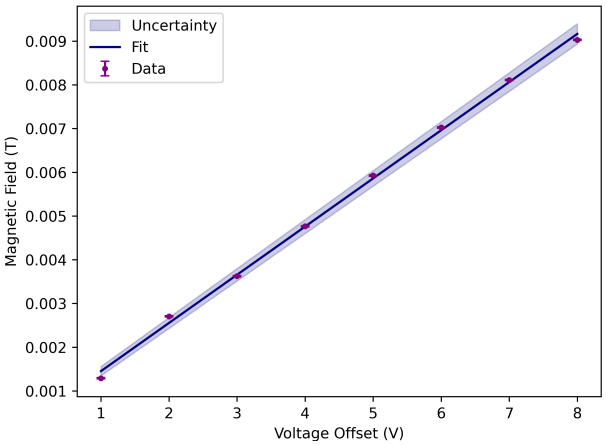

(b)

Figure 5: *Magnetic field strength in tesla versus offset voltages in* 1.00*V increments. (a) First determination with offset voltage range of* 1.00-7.00*V with weighted linear regression equation of* $B_0 = (1.172 \cdot 10^{-3} \pm 8.689 \cdot 10^{-3} V) + (-5.357 \cdot 10^{-5} \pm 3.886 \cdot 10^{-5})$*, and (b) second determination* 1.00-8.00*V with weighted linear regression equation of* $B_0 = (1.102 \cdot 10^{-3} \pm 1.769 \cdot 10^{-5} V) + (3.505 \cdot 10^{-4} \pm 8.933 \cdot 10^{-5})$.

Resonance voltage measurements for the first determination saw voltage uncertainties in the range of ±0.01 – 0.03V, though, uncertainties of ±0.01V were observed for all frequencies except for 160, 170, and 180MHz with respective uncertainties of ±0.02, ±0.03, and ±0.02V.

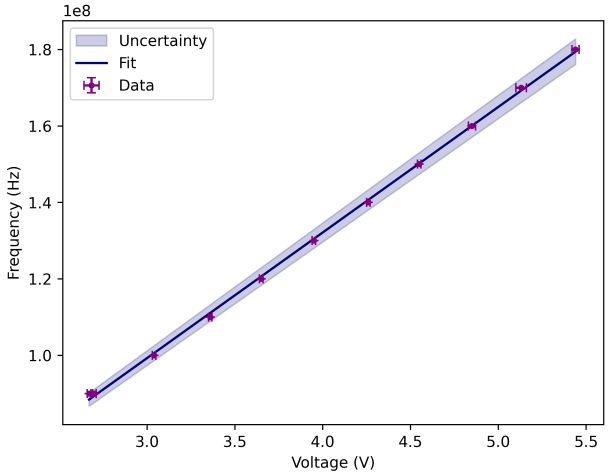

Figure 6: *Frequency in Hertz versus voltage offset in V for first determination with ODR slope equation of* $\omega = (3.285 \cdot 10^7 \pm 5.752 \cdot 10^5 V) + (6.932 \cdot 10^5 \pm 2.016 \cdot 10^5)$.

Resonant voltages from the lock-in amplifier must be determined before a relationship between the voltage and frequency can be made. This was accomplished by parsing through the .lvm files with Python, a constant offset voltage uncertainty of ±0.01V was assumed.

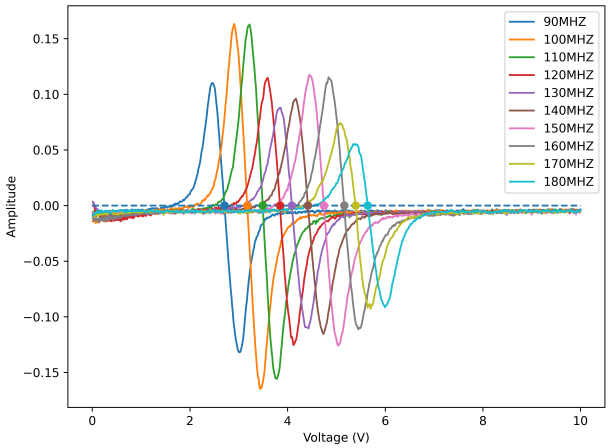

Figure 7: *Resonance voltage intercept plot representing the first derivative of the resonance absorption signal for second determination in the frequency range of* 90-180*MHz in* 10*MHz increments. Corresponding resonance offset voltage values were found to be* 2.707, 3.173, 3.491, 3.844, 4.087, 4.417, 4.72, 4.744, 5.160, 5.395, *and* 5.642*V, all with uncertainties of* ±0.01*V.*

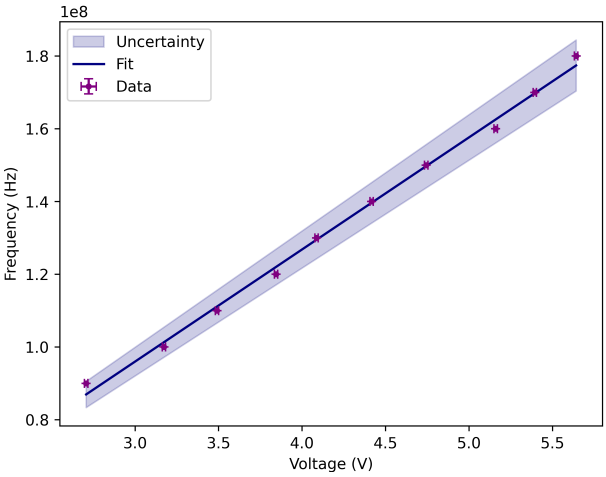

Figure 8: *Frequency in Hertz versus voltage offset in V for second determination with ODR slope equation of* $\omega = (3.082 \cdot 10^7 \pm 1.159 \cdot 10^6 V) + (3.507 \cdot 10^6 \pm 4.665 \cdot 10^5)$. *Offset voltage values were determined via finding the intercept offset voltage value of the first derivative of the resonant absorption signal.*

As predicted, the functions for the effective magnetic field strength and the corresponding resonant frequency have a linear relationship that can be exploited. This allowed (Eq. 2.3) to be manipulated into a plot of figure 5a versus figure 6 as well as figure 5b versus figure 8 for the first and second determinations respectively. The resulting slope is the predicted isotropic Landé g-factor for the sample of DPPH.

We find the slopes produced via linear regression in figure 9a and 9b provide values of 2.003 ± 0.017 from and 1.999 ± 0.053 for the isotropic Landé g-factor of DPPH. The first value agrees tremendously with the accepted value of $g = 2.0036$[5], differing only by 0.029%. The second value, while less, accurate, is still within uncertainty, differing by 0.23%. Despite undergoing a nearly identical data analysis process, the second determination of the g-factor is almost off by an entire order of magnitude, with an error 3.15 times larger when compared to the first determination even though the lock-in amplifier is far more sensitive to the resonant absorption signal.

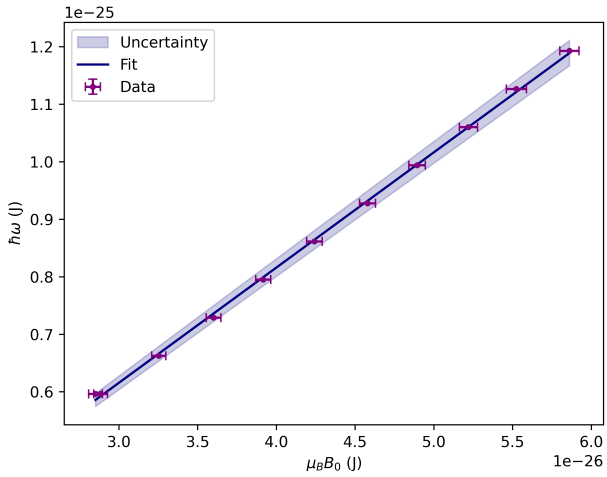

(a)

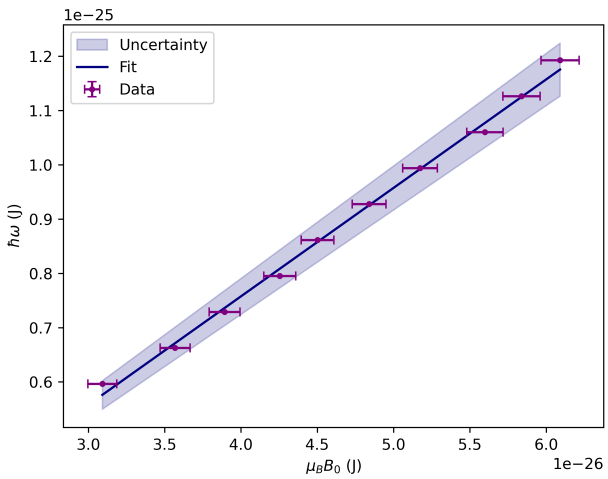

(b)

Figure 9: *Isotropic Landé g-factor for DPPH as slope value determined via ODR and multiplied by the scaling factors of h for the y-axis and* μ_B *for the x-axis from (a) the first determination with slope of* 2.003 ± 0.017, *and (b), the second determination with slope of* 1.999 ± 0.053.

This magnitude of error is predicted to be mainly due to not giving the Helmholtz coils any time to cool down during offset voltage sweep measurements as this was at least partially controlled for in the measurements used in the first determination. Additionally, the resonance absorption intercept points are prone to a large amount of error with how steep the slope can be as seen in figure 7. Increases of resistance within the Helmholtz coils appears to be the largest source of error in this experiment, affecting nearly every facet of it.

Because we were unable to contain either the Gaussmeter or variable capacitor probes

sufficiently near the sample, the Gaussmeter is not reading as accurate of an effective magnetic field strength as it could. The capacitor may not be tuned to the right capacitance either for the same reason on top of the tuning process being entirely dependent on the ability to estimate the minimum voltage by eye rather than an actual voltage reading.

6 Future Improvements and Works

In a repeated experiment to measure the isotropic Landé g-factor, it would be more conducive to focus on lower magnetic field strengths and resonant frequencies as these require less voltage to be put through the Helmholtz coils, reducing potential systemic error. The resonance offset voltage sweeps completed for the second determination would also greatly benefit from a longer duration such as 10 minutes or longer to more precisely determine intercept points. Other methods of dealing with heat include modifying $Eq.2.3$ for the effective magnetic field by adding a temperature dependence term to the equation that would be proportional to the offset voltage, accounting for the source of error intrinsically. A far more powerful cooling apparatus would also be of benefit, removing temperature dependence entirely within the voltage range used in this experiment. Digital microelectromechanics systems (MEMS) based variable capacitors and Gaussmeters have been around for decades, MEMS based Gaussmeters can be precise to the order of microtesla or even nanotesla, and can also be extraordinarily cheap depending on the model employed. Both of these could be placed almost directly where the sample lies, having their measurements sent and calibrating them via a microcontroller which can interface directly to a computer.

To observe even more pronounced ESR effects such as an anisotropic Landé g-tensor (Eq. 2.4), magnetic field strengths many orders of magnitude greater than the scale used in this experiment would be required, paired with a cooling system and measurement devices that are equally as robust. Analysis of DPPH in solution should also be considered because of its highly planar nature in solution.[6] Molecular dynamics and structure are hypothesized to behave completely differently due to potential ring currents being produced by the Phenyl and picryl groups of the molecule. These ring currents have the ability to greatly alter the spin density throughout the DPPH molecule as the magnetic field produced by the ring currents can either shield the electron from the external field or amplify it depending on whether or not the electron is more likely to sit within or outside of the phenyl and picryl groups.[7] We hypothesize that the electron would be confined to the hydrazyl group due to the ring currents. While a shielding effect that reduces the effective magnetic field is normally seen for protons within an aromatic group and an amplification outside of it in nuclear magnetic resonance experiments, the opposite would be true for an electron due to its negative charge. This would cause the effective magnetic field strength near the hydrazyl group to be reduced, resulting in a lower magnetic dipole potential energy within the area. A preliminary investigation assuming minimal coupling of the phenyl and picryl groups' molecular orbitals allows the application of the quantum continuity equation. A spacially invariant magnetic field $B_0\hat{z}$ can be transfomred into a magnetic vector potential under the Coulomb guage condition $\vec{\nabla}\cdot\vec{A}=0$ which results in

$$\vec{A} = \frac{r\sin(\theta)}{2}B_0\hat{\varphi}. \tag{6.1}$$

The qunatum continuity equation with the previously determined vector potential is then defined as[4]

$$\vec{J} = \frac{q}{2m}\left[\left(\langle\psi|\left(-i\hbar\vec{\nabla}\right)|\psi\rangle - |\psi\rangle\left(-i\hbar\vec{\nabla}\right)\langle\psi|\right) - 2q\vec{A}\langle\psi|\psi\rangle\right]. \tag{6.2}$$

Using linear combination of atomic orbitals (LCAO)s theory[4] and a basis set of STOs with real spherical harmonics to approximate each carbon's wave function in the aromatic ring allows us construct a molecular orbital wavefunction.[2][9] As a consequence of the real spherical harmonics, the complex conjugate

of the wave function is the same in all cases, therefore, (Eq. 6.2) can be reduced to.

$$\vec{J} = \frac{-q^2}{m}\vec{A}\langle\psi\,|\psi\rangle \tag{6.3}$$

From this an orbital angular momentum can be defined using the probability current density function from (Eq. 6.3)[4] as

$$\vec{L} = m\int_V (\hat{r} \times \vec{J})d\tau. \tag{6.4}$$

This orbital angular momentum creates a dipole moment and an associated magnetic field which is opposite in direction to the externally applied magnetic field and directly depends on the external fields magnitude. This phenomenon however, was not present in this experiment due to not recording any magnetic field strength measurements without the sample of DPPH. It is also hypothesized that because, DPPH's solid, crystaline state, orients its phenyl and picryl groups almost orthogonal to each other[5][6], Any external field that isn't oriented perfectly to the planar axis of one of the groups the magnetic fields created cancel each other out. While this does hold true, it's also simultaneously in the form of a powder, meaning that every molecule is, for all intents and purposes, oriented randomly, cancelling out any molecular magnetic field effects that depend on any form of axial symmetry.

While the spin density function for DPPH can be approximated quite well as see in in figure 2, a far more complex model is required to apply any concepts in molecular dynamics as the spin density function is, unfortunately, just an expectation value.[6] The next iteration of computational analysis of DPPH would be to construct its molecular orbital wave function. This would be accomplished in a similar manner to how the spin density function was defined with linear combinations of STOs though, in a slightly more nuanced manner. This includes creating a basis set or a set of basis functions, where multi-electronic atomic wave functions are approximated to be linear combinations of these basis functions.[2][9] We hypothesize the use of a STO basis with six different zeta functions for each orbital level l for each element in the molecule which then has its parameters optimized via the Hartree-Fock algorithm.[9] After each approximate atomic orbital wave function is optimized, the DPPH molecule can be approximated to be LCAOs comprised of STOs itself which is again optimized using the Hartree-Fock algorithm.[9] First or potentially second order perturbations could then be applied for corrections such as the spin-orbit interaction and dipole-dipole interactions.[4] The process of optimization for the wave function of a single light atom is extremely computationally intensive, requiring overlap integrals for each STO present in the approximated wave function along with expectation values for their kinetic and potential energies. This is further complicated when considering molecular orbital wave function overlap integrals due to the varying distances between atomic centers which break symmetries used to compute integrals more easily. Because of this, any molecular overlap, kinetic energy, or potential energy integrals would need to be done numerically and are extremely computationally expensive. The parallelization of computations via GPU hardware acceleration demonstrates its effectiveness as well as its key role in approximating DPPH's molecular wave function, especially as GPUs are extremely proficient at matrix operations which is the core of the Hartree-Fock algorithm.

7 conclusion

In this study, we successfully determined the isotropic Landé g-factor for diphenylpicrylhydrazyl (DPPH) through electron spin resonance (ESR) spectroscopy, achieving values of 2.003 ± 0.017 and 1.999 ± 0.053 using two distinct measurement methods. The first determination demonstrated remarkable agreement with the accepted value of $g = 2.0036$[5], differing by only 0.029%, while the second determination, though less precise with a 0.23% difference, still fell within uncertainty margins.

Our analysis of DPPH's spin density distribution confirmed the molecule's suitability for ESR measurements due to its orbital quenching properties, which result in an effectively free electron that can be studied with relatively simple apparatus.[5] The computational model we developed using GPU-accelerated processing allowed us to visualize the electron's probability density throughout the molecule, providing insight into the physical basis for DPPH's nearly isotropic Landé g-factor at the frequencies used in our experiment.[6]

Despite equipment limitations and thermal management challenges, our methodology proved robust enough to yield highly accurate results. Future improvements should focus on enhanced cooling mechanisms for the Helmholtz coils, integration of MEMS-based sensors for precise field measurements, and extended data acquisition times to reduce noise. Additionally, exploring anisotropic g-tensor effects in oriented DPPH crystals or solution-phase studies could provide deeper insights into molecular dynamics and shielding effects induced by aromatic ring currents.[6][7][11] The success of GPU-accelerated computational methods in modeling spin density underscores their critical role in advancing molecular orbital wave functions simulations for complex systems like DPPH.

This study demonstrates the continued relevance of ESR spectroscopy in undergraduate physics education, providing students with practical experience in quantum mechanics, electromagnetic theory, and experimental methods. The combination of experimental and computational approaches used here represents a comprehensive framework for investigating electron properties in complex molecular systems.

Acknowledgements

I would like to thank Troy Brajcic, Jakob Untch, Sebastian Ruiz-Huidobro, Serena Bengert, Nix Dhanbir, Daniel Nixon, and Dante Kelley for their technical guidance and moral support throughout the strenuous development of this text.

References

[1] A. Abragam and B. Bleaney. *Electron Paramagnetic Resonance of Transition Ions*. Vol. 48. Clarendon Press, 1970. ISBN: 978-0-19-965152-8.

[2] Ignacio Ema et al. "Polarized basis sets of Slater-type orbitals: H to Ne atoms". In: *Journal of computational chemistry* 24 (June 2003), pp. 859–68. DOI: 10.1002/jcc.10227.

[3] X. Fan et al. "Measurement of the Electron Magnetic Moment". In: *Phys. Rev. Lett.* 130 (7 Feb. 2023), p. 071801. DOI: 10.1103/PhysRevLett.130.071801. URL: https://link.aps.org/doi/10.1103/PhysRevLett.130.071801.

[4] David J. Griffiths and Darrell F. Schroeter. *Introduction to Quantum Mechanics*. 3rd ed. Cambridge University Press, 2018.

[5] Petre Ionita. "The Chemistry of DPPH· Free Radical and Congeners". In: *International Journal of Molecular Sciences* 22 (Feb. 2021), p. 1545. DOI: 10.3390/ijms22041545.

[6] J. Maruani J.X. Boucherle B. Gillon and J. Schweizer. "Spin distribution in the diphenylpicrylhydrazyl (DPPH) radical measured by neutron diffraction". In: *Molecular Physics* 60.5 (1987), pp. 1121–1142. DOI: 10.1080/00268978700100751. eprint: https://doi.org/10.1080/00268978700100751. URL:

https://doi.org/10.1080/00268978700100751.

[7] Jonas JuséLius and Dage Sundholm. "Ab initio determination of the induced ring current in aromatic molecules". In: *Physical Chemistry Chemical Physics - PHYS CHEM CHEM PHYS* 1 (Aug. 1999), pp. 3429–3435. DOI: 10.1039/a903847g.

[8] Igor Khudyakov, Yuri Serebrennikov, and Nicholas Turro. "Spin-orbit coupling in free-radical reactions: On the way to heavy elements". In: *Chemical Reviews* 93 (Jan. 1993). DOI: 10.1021/cr00017a023.

[9] R. Krishnan et al. "Self-consistent molecular orbital methods. XX. A basis set for correlated wave functions". In: *The Journal of Chemical Physics* 72.1 (Jan. 1980), pp. 650–654. ISSN: 0021-9606. DOI: 10.1063/1.438955. eprint: https://pubs.aip.org/aip/jcp/article-pdf/72/1/650/18920563/650_1_online.pdf. URL: https://doi.org/10.1063/1.438955.

[10] Harold M. Swartz. "Electron Spin Resonance: A Comprehensive Treatise on Experimental Techniques by C. P. Poole, Jr." In: *Medical Physics* 11.4 (1984), pp. 568–569. DOI: https://doi.org/10.1118/1.595516. eprint: https://aapm.onlinelibrary.wiley.com/doi/pdf/10.1118/1.595516. URL: https://aapm.onlinelibrary.wiley.com/doi/abs/10.1118/1.595516.

[11] J.A. Weil and J.R. Bolton. *Electron Paramagnetic Resonance: Elementary Theory and Practical Applications, Second Edition*. Vol. 48. 2007. ISBN: 978-0471-75496-1. DOI: 10.1063/1.2808029.

Appendix

Code used for DPPH electron spin density approximation and graphics can be found here.

Code and data used in the determination of DPPH's Landé g-factor and corresponding graphics can be found here.